Science of the Total Environment 1006 (2025) 180925

Contents lists available at ScienceDirect

Science of the Total Environment

journal homepage: www.elsevier.com/locate/scitotenv

Research Paper

Five decades of groundwater change across a diverse Mediterranean climate region: Disentangling natural and human drivers of water quantity and quality

Diogo Costa [a,b,c,*], João Santos [b,d], António Chambel [e]

[a] MED – Mediterranean Institute for Agriculture, Environment and Development & CHANGE – Global Change and Sustainability Institute, Department of Geosciences, Universidade de Évora, Pólo da Mitra, Ap. 94, 7006-554 Évora, Portugal
[b] CREATE – Center for Sci-Tech Research in Earth System and Energy, Universidade de Évora, 7000-671, Évora, Portugal
[c] University of Saskatchewan, Department of Geography and Planning, 105 Administration Pl, Saskatoon, SK S7N 5A2, Canada
[d] Escola Superior de Tecnologia e Gestão, Instituto Politécnico de Beja, R. Pedro Soares S/N, 7800-295, Beja, Portugal
[e] Instituto de Ciências da Terra (ICT), Universidade de Évora, 7000-671, Évora, Portugal

GRAPHICAL ABSTRACT

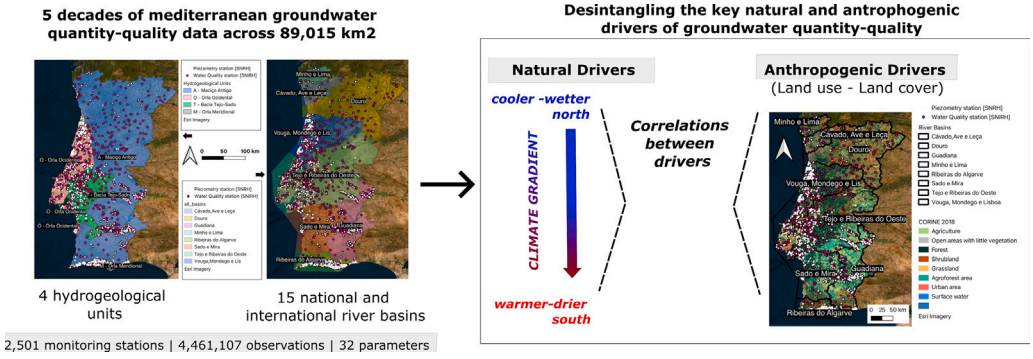

HIGHLIGHTS

- Large-scale groundwater study covering 89,015 km^2 of a Mediterranean climate region.
- Spatial aggregation in 4 hydrogeological units, 15 basins, using 4.4M observations.
- Temperature-driven mineral dissolution and geology shape north–south water quality patterns.
- Agriculture and forests strongly affect increases and drops in water quality, respectively.
- Intensive irrigation in southern areas causes groundwater depletion and nitrate rise.

ARTICLE INFO

Keywords:
Groundwater
Long-term monitoring
Decadal trends
Regional drivers of pollution

ABSTRACT

Groundwater systems in Mediterranean regions are under increasing pressure from climate variability and human activities, yet long-term, large-scale assessments of water quality dynamics remain scarce. This study compiles and analyses over 4.4 million observations collected from 2,501 monitoring stations across Portugal, covering an area of 89,015 km^2 over a 3.5-decade period (1970–2024), and encompassing 15 national and international river basins as well as four major hydrogeological units. Using custom data extraction workflows and spatial-statistical methods, we explored trends and patterns along climatic gradients, seasonal cycles, and

* Corresponding author.
E-mail address: diogo.costa@uevora.pt (D. Costa).

https://doi.org/10.1016/j.scitotenv.2025.180925
Received 3 June 2025; Received in revised form 17 October 2025; Accepted 6 November 2025

Surface-groundwater interactions

land use types, focusing on 32 groundwater quality parameters spanning physicochemical, microbiological, and nutrient indicators. Results reveal consistent large-scale north-to-south groundwater quality degradation gradients. This pattern could be partially explained by the geology and effect of temperature on rock-water interactions, increasing mineral dissolution, particularly for calcium, sodium, and magnesium. In contrast, parameters more affected by large-scale land use patterns, such as nitrates, chlorides, and potassium, showed a weaker response to the climate gradient, and their concentrations were more closely correlated to anthropogenic activities, with higher levels typically associated with agricultural, pastoral, and urban land uses. These findings reveal that groundwater is already showing signs of degradation linked to agricultural activities. This underscores the need for integrated monitoring frameworks that consider both climatic and land use drivers, enabling more targeted protection and restoration efforts in Mediterranean groundwater systems.

1. Introduction

Throughout the world, groundwater is a strategic resource, playing an important role in water supply to populations, economic development, and in the support of sensitive ecosystems, especially during periods of drought (Frappart and Merwade, 2022; Chung et al., 2023; Shaikh and Birajdar, 2024). Groundwater constitutes approximately 30% of the world's freshwater resources, serving as a crucial source for domestic, agricultural, and industrial needs (Frappart and Merwade, 2022), and in many regions, especially semi-arid areas, groundwater is often the last available freshwater source. For example, in Europe, groundwater provides 65% of drinking water and 25% of water for irrigated agriculture in the 27 EU Member States (EU—27), and yet good status has not been achieved for all EU groundwater bodies (European Environment Agency, 2022).

Climate change is already exacerbating existing problems related to water quality globally (Costa et al., 2022), with subtropical and Mediterranean regions identified as particularly vulnerable. In these regions, precipitation typically peaks during fall and winter, causing nutrients accumulated in the soil to be suddenly released into rivers, lakes, and groundwater, while climate change simultaneously intensifies drought conditions (Santos et al., 2025).

It is recognized that the quantity and quality of groundwater are influenced by a multitude of factors, from natural to anthropogenic, making the understanding of how factors interact critical for effective water management. For example, land use and land cover (LULC) play an important role in the status of groundwater systems, with agriculture practices increasing the risk of diffuse pollution (Meghanad et al., 2025), which, in combination with background natural drivers such as geological composition, seasonal climatic variations and biogeochemical processes, determine the state of the resource regionally and locally (Kaminsky et al., 2023; Kumar and Singh, 2024; Meghanad et al., 2025).

Around the world, significant efforts have been made to separate natural and anthropogenic factors influencing groundwater. In North America, in 1998, Kolpin et al. (1998) had already detected pesticides in over half of shallow groundwater sites across U.S. basins, highlighting land use impacts. More recently, Huang et al. (2018) showed that the impacts of extensive industrialization in the Pearl River Delta in southern China over the past three decades were linked to high levels of heavy metal(loid)s, and that nitrate contamination stems mainly from domestic sewage and industrial wastewater leakage. It was also found that anthropogenic and natural processes are the factors that influence the chemical dynamics of groundwater in the urbanized areas of this delta region (Huang et al., 2013), inducing changes in groundwater quality of both granular and fissured aquifers (Zhang et al., 2019).

In Europe, several studies have also attempted to achieve the same goal, with Abduljaleel et al. (2024) finding that afforestation and urban expansion in Hungary's Drava floodplain (1990–2018) reduced groundwater recharge and levels. Patekar et al. (2021) reported that intensive agriculture and fertilizer use are degrading groundwater quality in karst catchments of southern Croatia. In Denmark, Foster and Bjerre (2022) identified intensive farming as a major source of nitrate leaching despite mitigation efforts. The combined effect of climate change and land use on a large groundwater reservoir in the Veluwe, The Netherlands, for a historical period (1850–2016) and in the future (2036–2065) was studied by Van Huijgevoort et al. (2020), identifying changes in recharge rates, evaporation, and contamination levels.

In southern Portugal, Penha et al. (2016) demonstrated that agricultural areas contribute to elevated nitrate concentrations in groundwater, while urban areas increase chloride and sodium levels, underscoring the role of land use in shaping groundwater chemistry. Samples from six groundwater wells with different land uses were analysed, and correlations were established between olive groves and vineyards and high levels of different physical and chemical parameters, demonstrating that various LULCs influence water quality in different ways. Zeferino et al. (2021) also assessed groundwater quality in a northern coastal region of Portugal, the Esposende-Vila do Conde nitrate vulnerable zone, revealing that despite existing nitrogen-reducing measures, nitrate concentrations above 50 mg/L are expected to persist over the next two decades due to agricultural nitrogen loads and nutrient legacy. Mansilha et al. (2020) studied the chemistry of several springs connected to small public water supply systems in a peri-urban area in northern Portugal, following a major forest fire in October 2017. High levels of sulphate, fluoride, nitrogen, and pH variability were detected, along with high concentrations of iron, manganese, and chromium, particularly after precipitation events.

Although regional and local studies on groundwater dynamics are relatively abundant throughout Europe and, to some extent, in Portugal, comprehensive, large-scale, long-term investigations at the national level remain remarkably limited, particularly in Mediterranean regions, where climate change is expected to intensify water quality degradation (Costa et al., 2022). Yet, such studies are paramount for underpinning effective nationwide strategies.

The study presented herein is the first one focusing on long-term trends in groundwater status across large Mediterranean climate and land-use gradients comprising the entire Portuguese continuum. One of the main limitations of existing studies in this region is the scarcity of concurrent quantity and quality records, which we address here by using comprehensive nationwide datasets. The results extend a previous study focused on surface water covering the same region (Costa et al., 2025). It is intended to be of practical value to water resource planning and management activities. It also aims to help increase stakeholder engagement by providing knowledge that can be used to create risk-based pollution management plans, as well as to understand the link between dominant factors and impacts.

2. Materials & methods

2.1. Study domain

This study focuses on groundwater bodies spanning across 4 major hydrogeological units and 15 national and international river basins within mainland Portugal, comprising a total area of 89,015 km^2. It uses a large national dataset supported by monitoring stations maintained by the Portuguese Environment Agency (APA). Fig. 1 presents the geographical distribution of the monitoring stations in relation

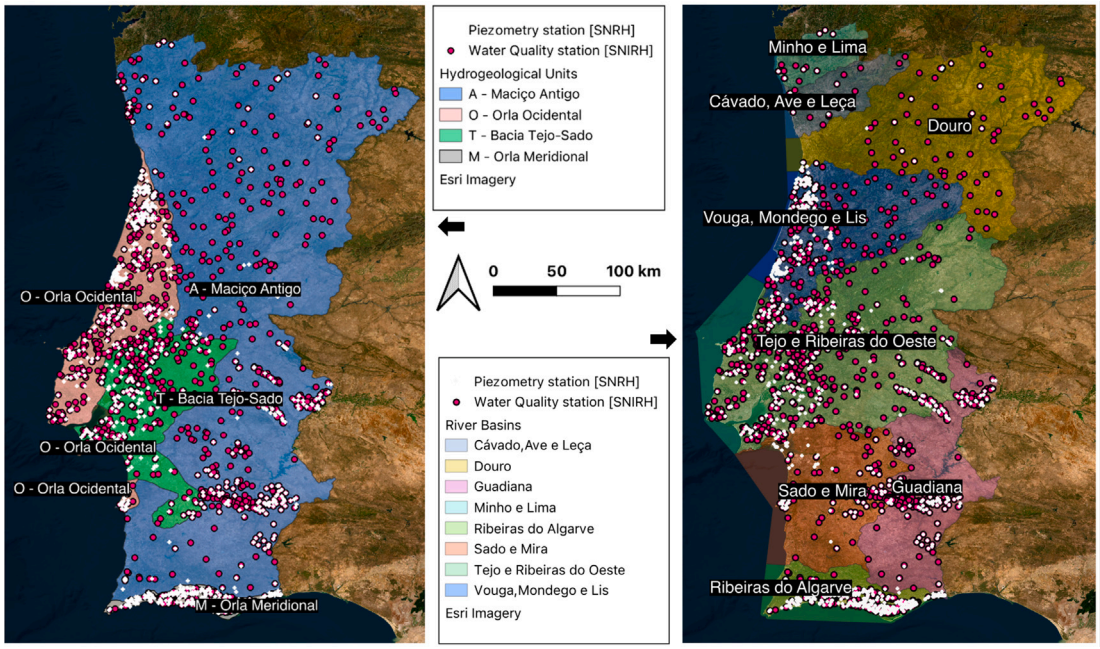

Fig. 1. Distribution of the observation stations/location (black and pink dots for water quantity and quality stations, respectively, with a total of 1018 and 1455 stations) overlayed on the main (sub-surface) hydrogeological units (left-panel) and (surface) river basins (right-panel). More details about the characteristics of this dataset are provided in Table 1.

to sub-surface (hydrogeological units; left–panel) and surface (river basins, right–panel) water systems. The large spatial and temporal coverage is critical to help disentangle sources and large-scale impacts of groundwater contamination.

The hydrogeological systems have been aggregated into four units, in line with the classifications officially recognized at national and European levels (Almeida et al., 2000): (a) Maciço Antigo, (b) Orla Ocidental, (c) Bacia Tejo-Sado, and (d) Orla Meridional. Each of these hydrological units consists of several aquifers and less productive zones, considered as non-aquifers, but with potential to support less demanding uses (e.g., little villages, individual houses, little gardens). Aquifer systems in Portugal are mainly porous and karst (Penha et al., 2016), with the porous environment being the most significant with an area of 26,000 km^2 (i.e., 29.4% of the national territory), followed by karst groundwater, which represents an area of 5,500 km^2 (i.e., 6.2%). The division into 4 hydrogeologic units (Almeida et al., 2000) is based on geology:

- Most of Portugal is underlain by igneous and metamorphic formations (Maciço Antigo), dominated by fractured aquifers. There are some karst systems and a sedimentary porous phreatic aquifer, but together they represent only about one percent of the total area of the Maciço Antigo unit.
- The Orla Ocidental (Western unit) is composed of sedimentary formations, containing 27 aquifer systems ranging in size from 5 to 931 km^2, alongside extensive areas considered non-aquifer. It includes recent detrital systems (Quaternary to Plio-Pleistocene porous multi-layer aquifers, ranging from phreatic to confined), older detrital systems (Miocene to Cretaceous, porous multi-layer aquifers, phreatic to confined), and carbonate aquifer systems (Jurassic karstic aquifers).
- The Orla Meridional (Southern unit) also consists of sedimentary formations, encompassing 17 aquifer systems ranging from 5.3 to 318 km^2, along with extensive areas considered non-aquifer. It includes detrital systems (Quaternary and Miocene, porous aquifers, phreatic to confined), carbonate formations (Jurassic and Cretaceous, karstic aquifers, phreatic to confined), and mixed systems (Quaternary to Jurassic, combining porous and karstic aquifers, phreatic to confined).
- The Tejo-Sado unit comprises 4 aquifer systems, ranging in size from 687 to 702 km^2, with only a small area at the basin margins considered non-aquifer. All four systems are multi-layered: three are hosted in sedimentary rocks (porous media), and one is a mixed formation, containing both karstic and porous media".

The scale of the aquifers highlights why the analysis should not be confined to basic hydrogeological units, some of which are as small as 5 km^2. Since the data are compiled at the national level, analysing individual aquifers would disperse much of the information across numerous small units, thereby weakening the robustness of the statistical analysis. Crucially, the data still reflect the same rock formations that define the aquifers, even if they correspond to less productive sectors.

The 15 river basins located in this area have been aggregated into eight broader clusters following the hydrographic regions implemented in Portugal within the European Water Framework Directive (WFD), i.e., smaller catchments have been grouped within larger adjacent river systems. The grouping is as follows: Minho and Lima (Cluster 1), Cávado, Ave, and Leça (Cluster 2), Douro (Cluster 3), Vouga, Mondego, and Lis (Cluster 4), Tejo and Ribeiras do Oeste (Cluster 5), Sado and Mira (Cluster 6), Guadiana (Cluster 7), and Ribeiras do Algarve (Cluster 8).

2.2. Long-term multi-parameter monitoring (1970–2024)

To characterize large-scale groundwater quality patterns across Portugal and disentangle natural from anthropogenic drivers for management purposes, we compiled an extensive national dataset from APA's publicly accessible databases, available through the National Water Resources Information System (SNIRH). Due to database system constraints limiting 50 station-parameter combinations per download, custom scripts were developed to automate and streamline data retrieval and processing, addressing a technical barrier that may partly explain the limited number of large-scale studies in the region. The full dataset is archived on ZENODO (https://doi.org/10.5281/zenodo.15472032), along with (i) the complete set of scripts for data extraction, processing, and compilation, and (ii) all figures in interactive

Table 1
Water quantity and quality parameters analysed. The frequency of the measurements is given in "days" and is the average calculated for all the stations for each parameter.

Parameter	# Stations	# Observations	Period	Frequency[a] (days)
QUANTITY				
Piezometric levels[b]	955	2122,656	[1969, 2024]	48
Water level depth	955	2122,656	[1969, 2024]	48
GENERAL				
Hardness	160	1644	[1996, 2024]	193
Total hardness (mg/L $CaCO_3$)	410	3537	[1990, 2020]	192
Total alkalinity (mg/L $CaCO_3$)	241	1816	[1990, 2020]	256
pH - lab.	880	15,427	[1992, 2024]	258
Conductivity (μS/cm)	374	3569	[1995, 2023]	201
Laboratory conductivity at 20 °C (μS/cm)	716	10,093	[1992, 2024]	284
Colour (mg/L Pt-Co)	131	1531	[1996, 2022]	254
Sample temperature (° C)	938	15,275	[1991, 2024]	266
Dissolved oxygen - field (mg/L O2)	249	2120	[1990, 2023]	343
Dissolved oxygen - field (%)	236	2049	[1996, 2023]	315
MICROBIOLOGY				
Total Coliforms CFU	773	4419	[2004, 2023]	232
Faecal coliforms UFC	768	4379	[1998, 2024]	228
Intestinal Enterococci (NMP/100 ml)	315	1895	[2011, 2024]	287
Faecal Streptococci	320	1465	[1999, 2024]	202
NUTRIENTS				
Nitrate (mg/L NO_3)	997	20,667	[1992, 2024]	217
Nitrite (mg/L NO_2)	911	15,611	[1993, 2024]	263
Ammoniacal Nitrogen (mg/L NH_4)	993	18,155	[1996, 2024]	237
Phosphate (mg/L PO_4)	247	1699	[1997, 2024]	184
Phosphate (mg/L P_2O_5)	833	11,758	[1996, 2021]	287
METALS				
Total iron (mg/L)	609	4757	[1998, 2023]	442
Dissolved iron (mg/L)	404	1771	[1998, 2021]	468
Total Manganese (mg/L)	508	3404	[1997, 2023]	460
Magnesium (mg/L)	545	3678	[1990, 2023]	241
OTHERS				
Chloride (mg/L)	958	17,435	[1990, 2023]	256
Calcium (mg/L)	567	4026	[1990, 2023]	254
Sulphate (mg/L)	930	15,992	[1990, 2023]	264
Sodium (mg/L)	257	1362	[1990, 2023]	252
Bicarbonato (mg/L)	323	3701	[1990, 2020]	218
Bicarbonate (mg/L)	340	1838	[1990, 2009]	216
Oxidizability to Permanganate (mg/L)	771	10,923	[1996, 2023]	259

[a] Average of the frequency of the measurements in the stations (days).
[b] The reference datum for the piezometric data is the average sea level.

HTML format. The data retrieval algorithms are also openly available at https://github.com/ue-hydro/eyedrop_data_extract.

The dataset spans observations from 1970 onward for quantity and 1990 onward for water quality, covering 2,501 monitoring stations or sampling points. It comprises over 36 parameters encompassing physicochemical indicators, potentially hazardous metals, organic pollutants, and microbiological elements. The dataset comprises a total of 4,461,107 recorded observations and it includes parameters on water quantity and quality, as outlined in Table 1. The reference datum for the piezometric data is the average sea level.

While all analyses were performed for all parameters and the result are available in the ZENODO dataset, for the sake of clarity and conciseness, only a subset of the results are presented here. The criteria for selection of the results to present were:

- Spatial and Temporal Data Coverage: Only parameters with sufficient temporal resolution and spatial representation across multiple basins were retained to ensure the robustness and validity of the study;
- Significance of Parameters: Priority was given to parameters that support an integrated assessment of groundwater quantity and quality, including microbiology, nutrients, and metals, enabling the detection of spatial variability across basins as well as long-term temporal trends over recent decades; and
- Contributing to disentangle natural from anthropogenic drivers: Focus was given to parameters that enable the separation of natural and anthropogenic sources, thereby supporting the development of effective nationwide management strategies.

2.3. Methodology

The methodology outlined below was applied to all 32 water quality parameters listed in Table 1. Although the complete set of results is available through the ZENODO repository, only a subset is presented in this paper. Geographic data were sourced from OpenStreetMap (Bennett, 2010).

2.3.1. Spatial patterns along the climate gradient

The groundwater data were examined using two spatial aggregation criteria: hydrogeological units and river basins. Both approaches aimed to identify spatiotemporal patterns on groundwater status. However, the hydrogeological unit-based analysis focused on distinguishing differences related to aquifer systems and geological formations, while the river basin-based analysis sought to elucidare the effects of river-aquifer interactions and differences in climatic conditions. All analyses followed a latitudinal gradient approach, spanning from north to south, to capture the influence of climate on regional groundwater quantity and quality patterns.

Given the extensive size of the dataset, conducting detailed quality control at the level of individual data points was not feasible. To mitigate the influence of outliers and ensure robust central tendency estimates, medians and percentiles were used. The aggregated analysis at the hydrogeological unit or basin level was organized by latitude and visualized through thematic maps and boxplots, showing the minimum, maximum, and interquartile ranges (25th, 50th, and 75th percentiles). Since observation stations varied in measurement frequency, operational duration, and data availability, with some decommissioned and

others more recently established (see Table 1), the symbol size in map scatter plots was scaled according to the volume of available data, thereby emphasizing records with greater temporal coverage.

2.3.2. Seasonal patterns: regional and climate effects

The Mediterranean climate is characterized by pronounced seasonality, with hot, arid summers and cool, precipitation–rich winters. To assess the impact of these seasonal patterns on groundwater status, the dataset, aggregated by hydrogeological units (HU) and river basins (RB), was split up into dry (May—September) and wet (October—April) seasons. This seasonal separation was applied consistently across all water quality parameters. To further explore the interplay between seasonal variability and latitudinal climatic gradients, the resulting data distributions were visualized using boxplots arranged along a north-to-south climatic continuum, following the approach of the previous analysis.

2.3.3. Multidecadal trends & inflection points

To examine the combined natural and anthropogenic influences on groundwater quality, the data were organized chronologically and aggregated into five-year intervals. Water quality trends were then analysed using boxplots, ordered by climatic gradient, parameter, and time period. This framework facilitated a comparative assessment of temporal variations in water quantity and quality across regions subject to differing climatic conditions. Detailed information on the number of observations and temporal coverage for each parameter and monitoring station is provided in Table 1.

2.3.4. Evaluating land use and land cover as predictors of groundwater quality in mediterranean regions

To assess the impact of LULC on groundwater quality, LULC percentages were calculated for each drainage basin associated with the 2,501 monitoring stations. All analyses were initially performed at both the hydrological unit and river basin levels to enable comparison between the two. However, for correlations with LULC, the use of hydrogeological units proved statistically unfeasible: while there are 2,501 drainage basins (drainage areas contributing to each monitoring station), there are only four hydrological units, making the analysis statistically unreliable. Consequently, and given our primary focus on the influence of land use on groundwater, the results are presented exclusively based on data aggregated at the drainage basin level.

Drainage basin delineation for all 2,501 monitoring sites was fully automated using a hybrid vector—raster approach as conventional Digital Terrain Model (DTM)-based methods were computationally prohibitive. This approach was based on algorithms developed by Heberger (2023) and utilizing MERIT-Hydro and MERIT-Basins datasets (Yamazaki et al., 2019). Despite known limitations in complex terrains, these datasets provided adequate accuracy, as confirmed by comparisons with established basin boundaries — the relative error in the drainage area is < 0.05 for 90% of Global Runoff Data Centre (GRDC) gauges (Yamazaki et al., 2019). Following delineation, LULC class coverage within each basin was quantified using the CORINE Land Cover dataset from 2018 (Feranec, 2016) - more details in Section 2.3.4. The extensive spatial intersections required a fully automated geospatial workflow. Fig. 2 shows a representative subset of stations, their basins, and associated LULC classifications. All code and tools developed are publicly available via the ZENODO repository.

For each of the 2,501 drainage basins corresponding to the monitoring stations, two primary metrics were derived: (1) the median concentration of each water quality parameter and (2) the proportional coverage of each LULC class. These metrics were used to evaluate the predictive capacity of LULC in explaining spatial variations in water quality across the eight hydrological clusters representing the 15 Mediterranean catchments analysed (see Section 2.1). The relationship was quantified using both Pearson's correlation coefficient (PCC; Eq. (1)) and Spearman's rank correlation coefficient (SRC; Eq. (2)).

Table 2
Percentage of each land use category throughout the study period.

Land use	Percentage of each LULC		
	1995	2007	2018
Agriculture	28.6	25.8	26.2
Forests	36.8	38.6	38.7
Shurbs	13.2	12.9	12.4
Agroforest	8.8	8.5	8.4
Pasture	6.5	6.8	6.4
Urban	3.9	4.9	5.2
Water bodies	1.3	1.6	1.7
Open space with little vegetation	0.7	0.7	0.7
Wetlands	0.3	0.3	0.3

While PCC assesses linear relationships, SRC captures monotonic relationships regardless of linearity, providing a more nuanced non-linear (potentially compounded) understanding of LULC impact on water quality.

$$\rho_{x,y} = \frac{cov(x,y)}{\sigma_x \sigma_y} \tag{1}$$

where ρ is the Pearson correlation coefficient, x is the percentage of LULC (e.g., agriculture, forest, etc.), y is the median of the water quality parameter value (e.g., concentration), $cov(x,y)$ is the covariance between variables x and y, and σ_x and σ_y are the standard deviations of variables x and y.

$$\rho = 1 - \frac{6\sum d_i^2}{n(n^2-1)} \tag{2}$$

where ρ is the Spearman's rank correlation coefficient, d_i is the difference between the two ranks of each observation, and n is the number of observations.

Although groundwater water quality data span 1990 to 2024, the correlation analysis uses median concentrations aggregated over this period and relates them to LULC from a single reference year, CORINE 2018. This choice is justified by the small percentage changes in LULC class proportions over the study period (Table 2), indicating that comparable results would be obtained if other years were used. The aggregation of the original CORINE LULC classes presented in Table 2 was used throughout this study.

3. Results

3.1. Spatial patterns along the climate gradient

Fig. 3 presents the median values of various groundwater quality parameters, including groundwater depths (panels a, b, c), water temperature (panels d, e, f), pH (panels g, h, i), and electrical conductivity (panels j, k, l). These parameters are shown as spatial maps (left panels), and are also aggregated by HU (middle panels) and RB (right panels). The hydrogeological units and river basins are ordered geographically from north to south, reflected from left to right on the x-axis. Maps display the spatial distribution of each parameter, with circle colour indicating median values and size representing the number of observations. Most boxplots use a logarithmic scale on the y-axis to improve redability.

The results reveal a clear southward increase in groundwater depth, particularly across the Orla Ocidental, Bacia Tejo-Sado, and Orla Meridional regions. An exception is seen in the Guadiana Basin, where water tables are higher, likely due to enhanced groundwater recharge from the Alqueva reservoir. A similar southward gradient is evident in median water temperature, average pH, and electrical conductivity, consistent across both aggregation methods—by hydrogeological unit (middle panels) and by river basin (right panels). These spatial patterns are more pronounced when data are aggregated by river basin.

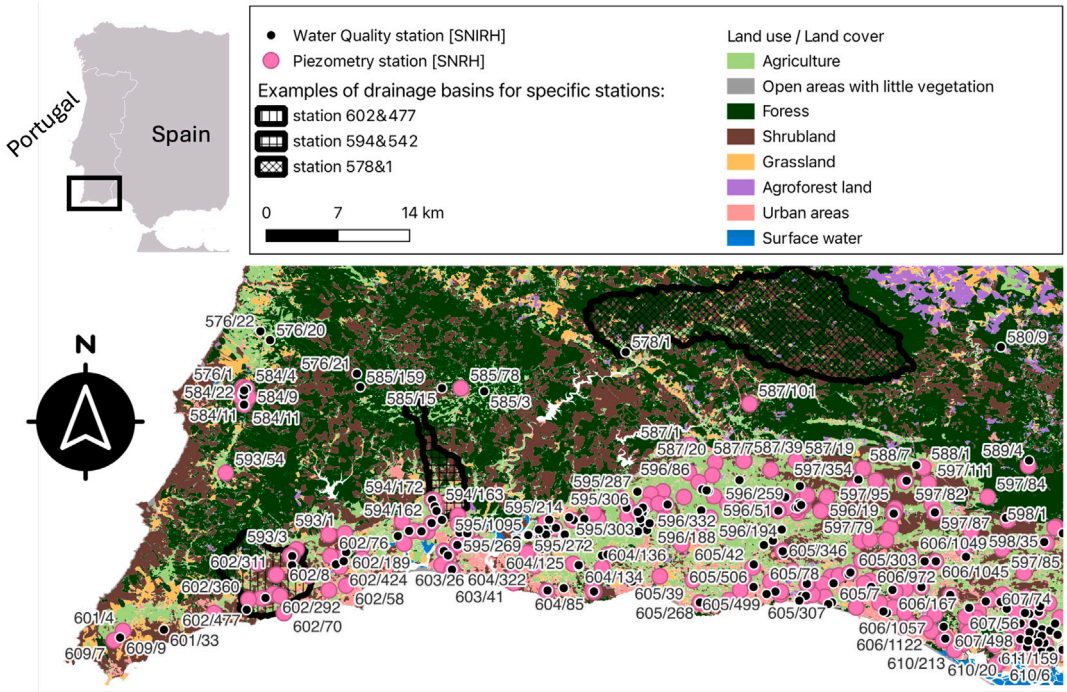

Fig. 2. LULC analyses involved delineating the drainage basins of all 2,501 stations or sampling locations involved in the study and determining the respective percentages of the different LULC types based on CORINE 2018.

Fig. 4 presents the results for major dissolved nutrients – nitrate (NO_3) and phosphate (P_2O_5) – as well as microbiological parameters, namely total and faecal coliforms. Concentrations of NO_3 and both coliform indicators remain relatively stable between the northern and central regions but show a consistent increase southwards, with the exception of the northern Cavado, Ave, and Leça river basins, which exhibit elevated values in the north. In contrast, phosphate displays the opposite pattern: concentrations remain stable up to the central regions but decrease progressively towards the south.

3.2. Seasonal patterns: regional and climate effects

Fig. 5 shows seasonal median values by basin for groundwater depth, temperature, and electrical conductivity. Fig. 6 presents the corresponding results for nutrient and microbiological indicators: nitrate, phosphate, total coliforms, and faecal coliforms. As expected, although only mildly, median water depths drop during the wet season. Temperature increases in the dry season, consistent with seasonal climatic patterns. Electrical conductivity, nitrate, and phosphate show minimal seasonal variation. In contrast, total and faecal coliform concentrations are low in the north and increase towards the south, with greater variability and higher peaks in the summer and towards the southernmost basin regions and hydrogeological unit (i.e., Orla Meridional).

Additional patterns, presented in Appendix, include a clear southward increase in most alkaline metal concentrations (sodium, magnesium, and calcium), with the exception of potassium, which shows the opposite trend (Fig. A.1). These patterns likely reflect underlying geological controls, potentially reinforced by climatic factors. Chloride and calcium carbonate also increase southwards, whereas total iron and sulphate do not display a consistent trend (Fig. A.2).

3.3. Multidecadal trends & inflection points

Fig. 7 illustrates the long-term trends of (a-b) groundwater depth, (c–d) electrical conductivity, (e–f) nitrate, and (g–h) phosphate. Parameters without clear temporal patterns have been excluded from the figure, but can be accessed through the ZENODO repository (see Section 2.2). Data are aggregated by hydrogeological units (left panels) and river basin groups (right panels) over the past 5 decades, with boxplots representing five-year intervals for each group. The bars represent the Q1, Q2, and Q3 quartiles. Outliers were excluded to enhance the interpretability of central tendencies, as some figures contain between 50 and 80 boxplots to illustrate decadal trends across regions.

Groundwater depths have remained relatively stable in the Orla Ocidental and Bacia Tejo-Sado, likely due to their proximity to the Atlantic Ocean and the major Tagus and Sado river systems. They have also remained stable in the Maciço Antigo. In contrast, the Orla Meridional in southern Portugal shows some evidence of aquifer depletion, with increasing groundwater depths (panel a and b), particularly noticeable in the last fifteen years (last three periods of the five-year intervals). Electrical conductivity has remained stable across most regions, but notable increases are observed also in the southernmost regions, specifically in the Orla Meridional (panel c) and in the Guadiana and Ribeiras do Algarve basins (panel d). In the latter, the simultaneous rise in EC and increase in water depths, suggests that aquifer depletion over the last decades may be potentially accompanied by saline intrusion from the Atantic Ocean on top of the already particularly high background concentration of alkaline metals in this region (see Appendix).

Since 2000, nitrate concentrations have declined in the Maciço Antigo and, to a lesser extent, in the Orla Meridional (panel e). Similar trends are observed when aggregating data by river basin (panel f), although the Guadiana River basin exhibits a slight increase up to 2020 before declining only more recently. Phosphate concentrations show no consistent long-term trend across either spatial aggregation; therefore, they are not shown here but are available in the ZENODO database.

3.4. Disentangling natural and anthropogenic drivers: The extent of LULC control on groundwater quality

Fig. 8 presents the PCC and SRC coefficients between the median concentration of different water quality parameters and the relative percentage area of different LULC. The results reveal positive PCC and SRC values for respectively 74% and 77% of the quality parameters (23 and 24 parameters out of 31) when related to the proportion of

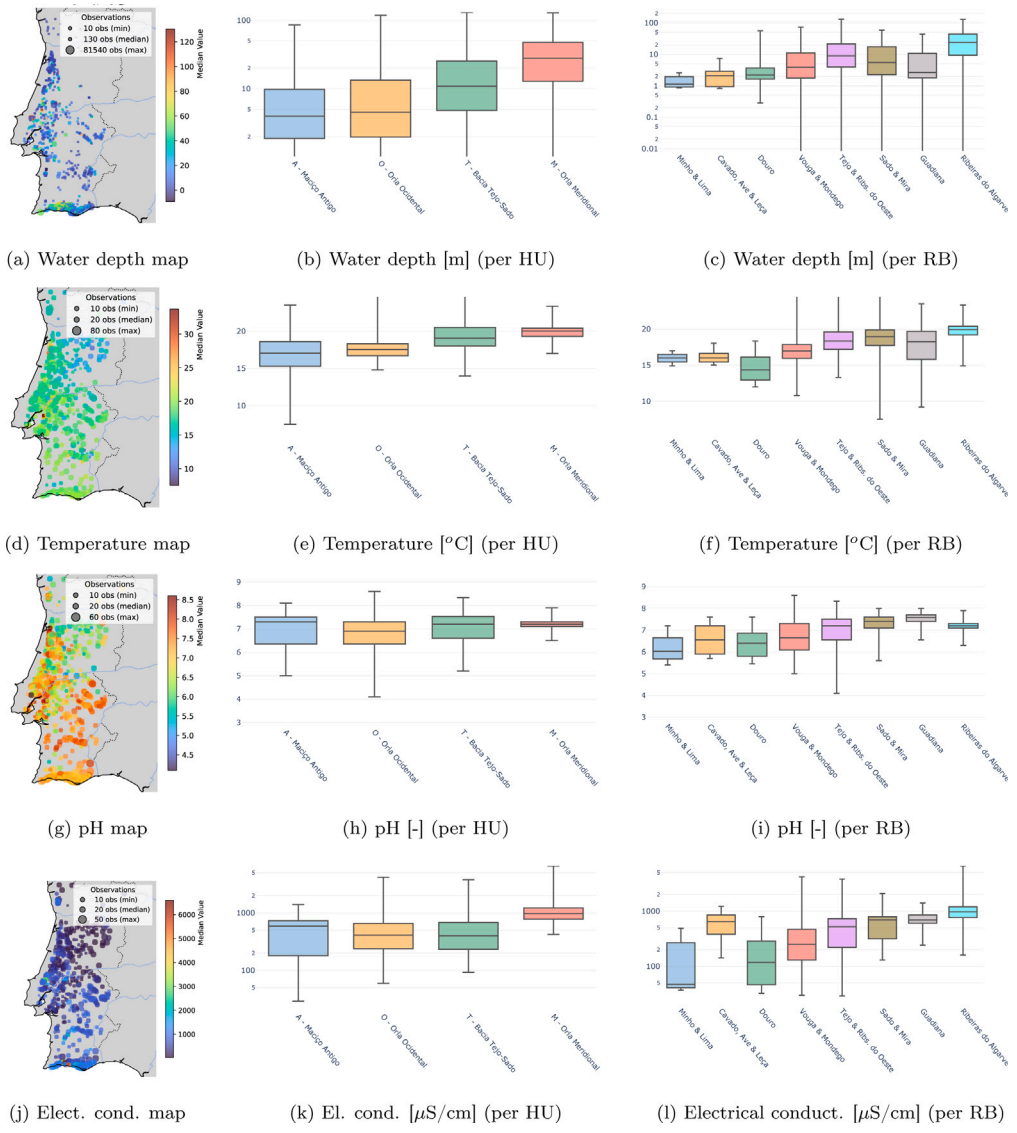

(a) Water depth map (b) Water depth [m] (per HU) (c) Water depth [m] (per RB)

(d) Temperature map (e) Temperature [^{o}C] (per HU) (f) Temperature [^{o}C] (per RB)

(g) pH map (h) pH [-] (per HU) (i) pH [-] (per RB)

(j) Elect. cond. map (k) El. cond. [μS/cm] (per HU) (l) Electrical conduct. [μS/cm] (per RB)

Fig. 3. Median values of groundwater depth [m], temperature [^{o}C], pH [-], and electrical conductivity [µS/cm] are shown as spatial maps (left panels) and boxplots aggregated by HU (middle panels) and RB (right panels). Maps display the spatial distribution of each parameter, with circle colour indicating median values and size representing the number of observations. Most boxplots use a logarithmic scale on the *y*-axis to improve redability. Aggregated groups are ordered along a north–south climatic gradient, from cooler, wetter regions to warmer, drier ones, reflected left to right on the *x*-axis.

agricultural land. The mean PCC and SRC values for the these positively related parameters are 0.23 and 0.31, with the highest correlations observed for Total Alkalinity (PCC = 0.54 and SRC = 0.49), Total Hardness (PCC = 0.39 and SRC = 0.43), Calcium (PCC = 0.44 and SRC = 0.50), pH (PCC = 0.40 and SRC = 0.40), Bicarbonate (PCC = 0.44 and SRC = 0.47), Magnesium (PCC = 0.41 and SRC = 0.48), Conductivity (PCC = 0.28 and SRC = 0.45), and Nitrate (PCC = 0.30 and SRC = 0.38). This trend indicates a general deterioration of groundwater quality with increasing agricultural land coverage. A similar, albeit weaker, trend is observed for bushland and grassland areas, where several water quality parameters also exhibit positive PCC and SRC values (highlighted as red cells in the heatmaps), suggesting a contribution to water quality degradation.

In contrast, forested areas exhibit a negative correlation with 77% and 81% of the water quality parameters for respectively the PCC and SRC (24 and 25 parameters out of 31), suggesting an overall improvement in groundwater quality with increasing forest cover. The mean PCC and SRC values for the these negatively related parameters are −0.25 and −0.36, with the highest negative correlations observed for Total alkalinity (PCC = −0.73 and SRC = −0.67), Total hardness (PCC = −0.60 and SRC = −0.58), Bicarbonate (PCC = −0.64 and SRC = −0.59), Calcium (PCC = −0.52 and SRC = −0.56), Magnesium (PCC = −0.45 and SRC = −0.54), Conductivity (PCC = −0.36 and SRC = −0,55), and Nitrate (PCC = −0.28 and SRC = −0.40).

Forests are widely recognized for their buffering capacity against contamination, helping to maintain and improve both surface and groundwater quality. Unlike agricultural areas, forests are also generally not subjected to large inputs of fertilizers, soil conditioners, or herbicides/pesticides. Notably, SRC values are generally higher than their PCC counterparts and are often associated with lower p-values, indicating greater statistical significance. This suggests that the relationships between LULC proportions and groundwater quality parameters are predominantly monotonic but not strictly linear.

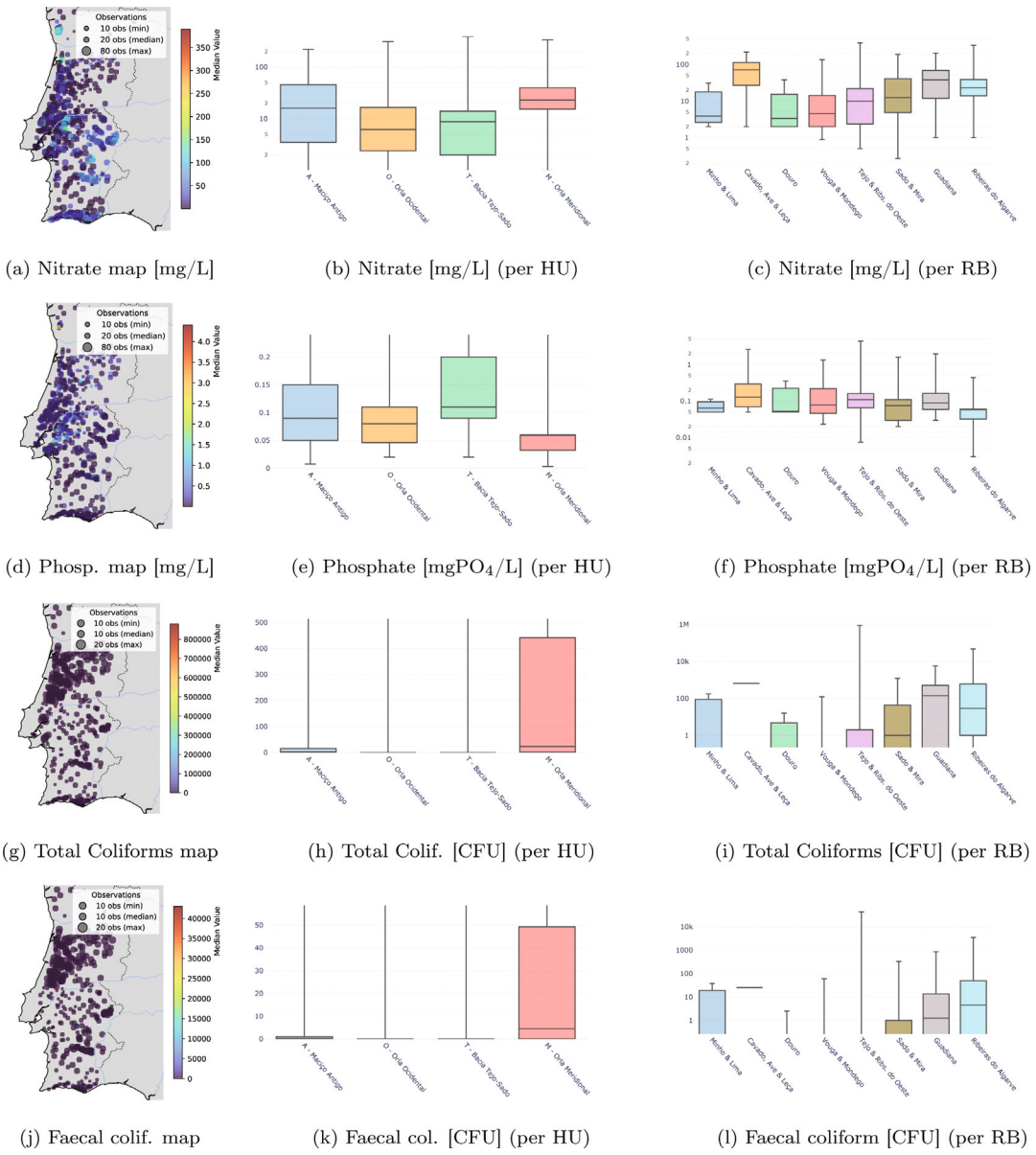

(a) Nitrate map [mg/L] (b) Nitrate [mg/L] (per HU) (c) Nitrate [mg/L] (per RB)

(d) Phosp. map [mg/L] (e) Phosphate [mgPO_4/L] (per HU) (f) Phosphate [mgPO_4/L] (per RB)

(g) Total Coliforms map (h) Total Colif. [CFU] (per HU) (i) Total Coliforms [CFU] (per RB)

(j) Faecal colif. map (k) Faecal col. [CFU] (per HU) (l) Faecal coliform [CFU] (per RB)

Fig. 4. Nitrate [mg/L], Phosphate [mgPO_4/L], total coliforms [CFU], and faecal coliforms [CFU] are shown as spatial maps (left panels) and boxplots aggregated by HU (middle panels) and RB (right panels). Maps display the spatial distribution of each parameter, with circle colour indicating median values and size representing the number of observations. Most boxplots use a logarithmic scale on the *y*-axis to improve redability. Aggregated groups are ordered along a north–south climatic gradient, from cooler, wetter regions to warmer, drier ones, reflected left to right on the *x*-axis.

4. Discussion

4.1. Disentangling climate-driven effects on water–rock interactions from land use-related contamination

Groundwater temperature is a key parameter that, in combination with regional differences in rock composition (ranging from acidic in the north to alkaline in the south), helps explain many of the observed water quality patterns. While this study does not allow a definitive separation of climatic drivers from other influencing factors, such as geology, limited recharge, and agricultural pressure, it provides valuable insights into their respective roles. To emphasize this, the x-axes of Figs. 3, 4, 5, 6, and 5, which represent the river basins or hydrogeological units, have been ordered along the north–south climate gradient (cooler–wetter to hotter–drier).

The results show that rising air temperatures from north to south lead to a corresponding increase in groundwater temperatures, which can, in turn, influence several water quality parameters, particularly those related to groundwater–rock interactions. Fig. 9 illustrates the temporal trend of groundwater temperature across all regions over recent decades, revealing a consistent warming pattern that may further intensify these interaction processes.

The thermodynamic conditions governing water–rock interactions promote increased mineral dissolution at higher water temperatures. The higher electrical conductivity (EC) values observed in the southern formations, along with the corresponding increases in calcium, sodium, and magnesium concentrations, suggest a climatic influence; however, these effects are likely intertwined with the underlying geology in shaping water quality. (Figs. 3 and A.1). In contrast, parameters more strongly influenced by land use, such as nitrates, chlorides, and potassium, exhibit a weaker response to the climate gradient (Figs. 4 and A.2). Their concentrations are instead more closely associated with anthropogenic activities, with higher levels more strongly correlated with agricultural, pastoral, and urban land uses (Fig. 8).

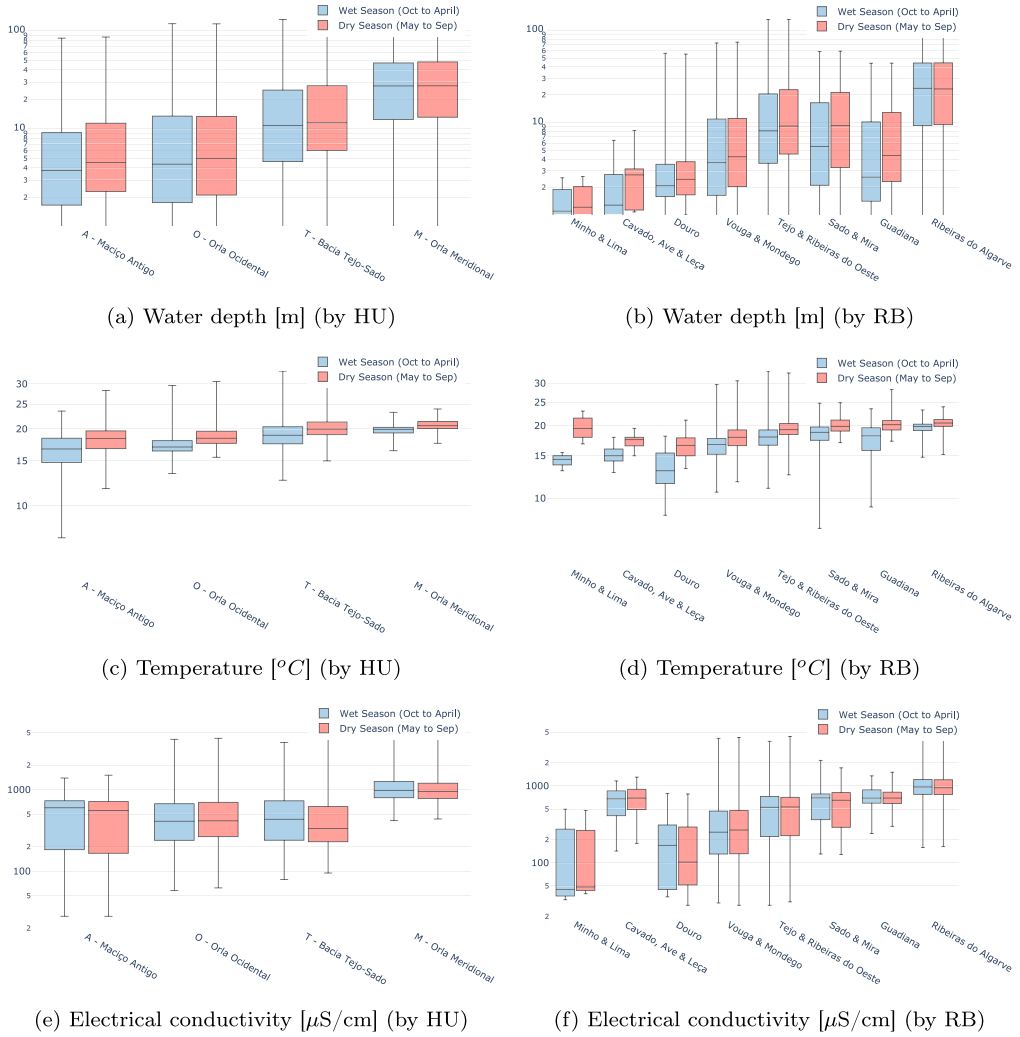

(a) Water depth [m] (by HU)

(b) Water depth [m] (by RB)

(c) Temperature [^oC] (by HU)

(d) Temperature [^oC] (by RB)

(e) Electrical conductivity [μS/cm] (by HU)

(f) Electrical conductivity [μS/cm] (by RB)

Fig. 5. Boxplots of seasonal concentrations are shown for (a-b) groundwater depth [m], (c–d) temperature [^oC], and (e–f) electrical conductivity [µS/cm], aggregated by hydrogeological units (left panels) and river basins (right panels). The x-axis represents four hydrogeological units or eight river basin groups, ordered geographically from north to south. The y-axis uses a logarithmic scale in most cases to improve redability.

4.2. Multidecadal trends in groundwater levels

The study reveals a drawdown of groundwater levels over recent decades which concurs with (a) a general reduction in precipitation in Portugal (Portela et al., 2020) leading to potential recharge reduction and (b) the expansion of intensive irrigation systems in this region (Eurostat, 2025) — Fig. 10 shows the increase in agricultural areas between 2007 and 2018 across most regions in Portugal. The increase in agricultural areas not only contributes to declining water levels but may also exacerbate contamination by nitrates and other agriculture — related pollutants through runoff export.

The downward trend in groundwater levels observed in recent years highlights a negative trajectory for groundwater sustainability, especially in the Algarve. This trend increases the risk of saline intrusion from the Atlantic Ocean, which may potentially be already happening given that this region presents the highest electrical conductivity levels across all regions and hydrogeological units. The study indicates a long-term decline in groundwater levels, coinciding with the expansion of intensive irrigation in Algarve (Eurostat, 2025). This expansion of irrigation not only lowers the water table but may also amplify contamination by nitrates and other agriculture-related pollutants through infiltration.

4.3. Can water quality patterns be linked to sources to inform management?

Geological patterns show more acidic rock formations in the north, transitioning to more basic formations towards the south. This gradient is reflected in the pH of groundwater, which aligns with the underlying lithological conditions (see metal and mineral concentrations in Appendix). The sources of phosphates can be natural, such as waterfowl waste, atmospheric deposition, weathering of geologic phosphate material, and plant decomposition; or they can be human-induced, such as agricultural fertilizer, animal waste, agricultural and urban runoff, industrial and domestic sewage, or faulty or overloaded septic systems. In Portugal, it is well established that there are not rocks with phosphates (Penha et al., 2016; Rocha et al., 2019), so they must be originated from contamination by agriculture and cattle production, with reduced dependency on climate rather than through controls on runoff intensity and consequent nutrient mobilization from soils.

Total coliforms and faecal coliforms are more dependent too of water temperature, which is higher in the southern part of Portugal and could partially explain the southward concentration increase (see Fig. 4), but they are also dependent on pollution by human and cattle intervention. As most part of these contaminants die in conditions of no light in a few days, their existence in groundwater means that the contamination is recent and can originate from domestic sewage systems.

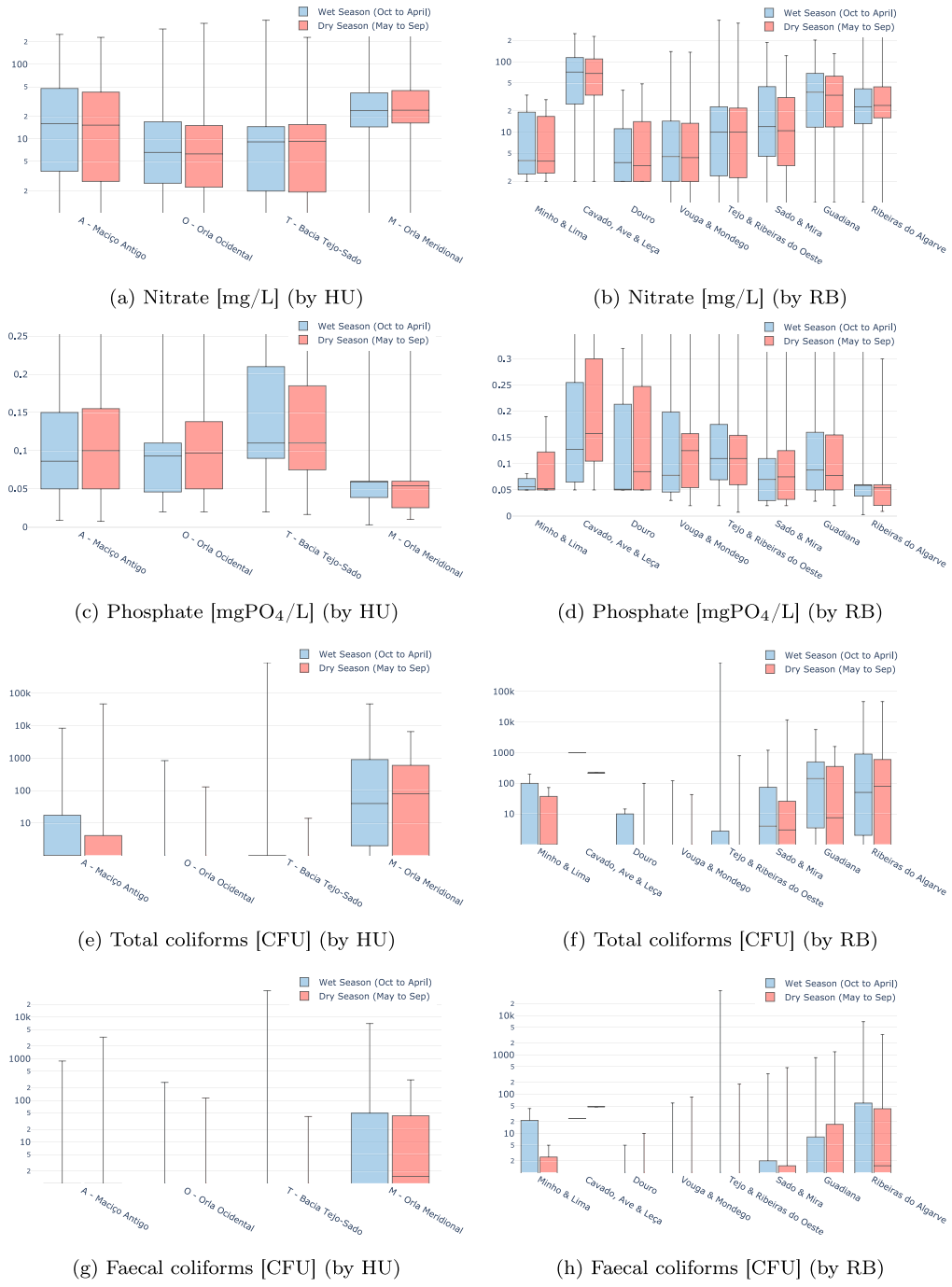

(a) Nitrate [mg/L] (by HU)

(b) Nitrate [mg/L] (by RB)

(c) Phosphate [mgPO_4/L] (by HU)

(d) Phosphate [mgPO_4/L] (by RB)

(e) Total coliforms [CFU] (by HU)

(f) Total coliforms [CFU] (by RB)

(g) Faecal coliforms [CFU] (by HU)

(h) Faecal coliforms [CFU] (by RB)

Fig. 6. Boxplots of seasonal concentrations are shown for (a–b) nitrate [mg/L], (c–d) phosphate [mgPO_4/L], (e–f) total coliforms [CFU], and (g–h) faecal coliforms [CFU], aggregated by hydrogeological units (left panels) and river basins (right panels). The *x*-axis displays four hydrogeological units or eight river basin groups, arranged geographically from north to south. The *y*-axis uses a logarithmic scale in most cases to improve redability.

4.4. Linking seasonal variations with underlying processes

Water table depths exhibit the expected seasonal dynamics of groundwater, with levels generally rising closer to the surface during the wet season relative to the dry season. Groundwater temperatures display a comparable seasonal trend, with higher values typically observed in the dry season. Electrical conductivity (EC), however, tends to be elevated during the wet season. This pattern may indicate that enhanced infiltration in the winter may exacerbate the leaching of contaminants and dissolved substances into the aquifer, potentially counteracting the dilution effect usually associated with rainfall.

This pattern is supported by seasonal variations in nitrate concentrations, one of the most mobile nutrients in the soil, which generally rise during the wet season; although some hydrogeological units and river basins exhibit the opposite trend, with higher concentrations in the dry season (see Fig. 5). Phosphate, another key pollutant, shows a similar dual behaviour: concentrations may increase during the wet season due to surface runoff, or become more concentrated in the dry season as a result of evapotranspiration.

Total and faecal coliforms also display seasonal variability, typically increasing during the wet season, likely due to enhanced surface infiltration carrying contaminants into the aquifer. In contrast, their presence diminishes in the dry season, as coliform bacteria tend to die

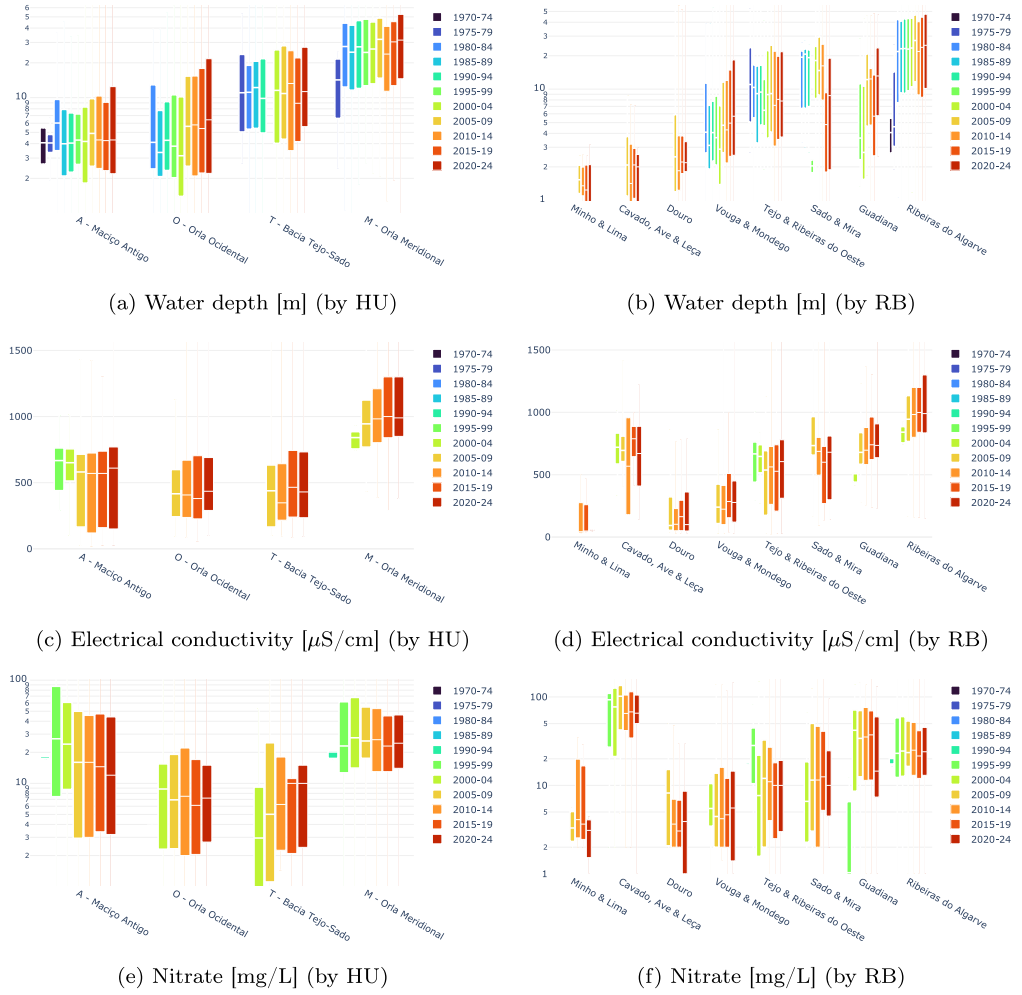

(a) Water depth [m] (by HU)

(b) Water depth [m] (by RB)

(c) Electrical conductivity [μS/cm] (by HU)

(d) Electrical conductivity [μS/cm] (by RB)

(e) Nitrate [mg/L] (by HU)

(f) Nitrate [mg/L] (by RB)

Fig. 7. Boxplots of observations from 1970 to 2024 are shown for (a-b) groundwater depth [m], (c–d) electrical conductivity [µS/cm], (e–f) nitrate [mg/L], and (g–h) phosphate [mgPO_4/L]. Data are aggregated by hydrogeological units (left panels) and river basin groups (right panels). The *x*-axis represents four hydrogeological units or eight river basin groups, ordered geographically from north to south.

off in dark, subsurface environments and are often retained within the vadose zone, limiting their transport into groundwater.

4.5. Five decades of change: Groundwater stress and shifting contamination trends

As shown in Fig. 7, groundwater depth has increased over the past 54 years across all hydrogeological units. This trend reflects the decrease in precipitation and intensifying exploitation of groundwater resources, primarily driven by agricultural demand. Over the same period, electrical conductivity (EC) has also risen, which can potentially be linked to a decline in water volumes leading to decreased dilution.

Nitrate exhibits a distinct temporal pattern over the past 55 years, with concentrations increasing until around 2000, followed by a general decline (panels e and f of Fig. 7). This shift likely results from multiple factors. The increase in irrigated land in Portugal, particularly in regions such as Alentejo, could be a determining factor, driven by projects such as the Alqueva Irrigation Project (do Nascimento et al., 2024). Before 2000, irrigation relied heavily on nitrate-rich groundwater; since then, reservoir water with lower nitrate levels has been increasingly used. Additionally, the introduction of modern irrigation technologies during this period, including computer-controlled systems and soil moisture sensors, likely reduced water losses, thereby minimizing fertilizer leaching into soils and, ultimately, into groundwater.

4.6. Limitations and prospects

While the availability of a robust dataset comprising 4.4 million observations collected over five decades represents a major strength of this research, it also poses challenges in ensuring the quality of all observation points. Comprehensive quality checks were not feasible; only spot checks could be conducted. To mitigate this limitation, medians rather than means were used in the analyses. Another constraint concerns the spatial distribution of observations: some regions, such as the Algarve, are densely monitored, whereas others, such as Maciço Antigo, are comparatively underrepresented.

To build on the findings presented, future research should further investigate the spatio-temporal variability of groundwater quality and quantity at the national scale, while also extending the analysis to the broader Iberian Peninsula, since most of the river basins considered are international, with Portugal being the downstream country. Particular attention should be given to understanding the influence of feedback between the natural and anthropogenic drivers. This effort may be

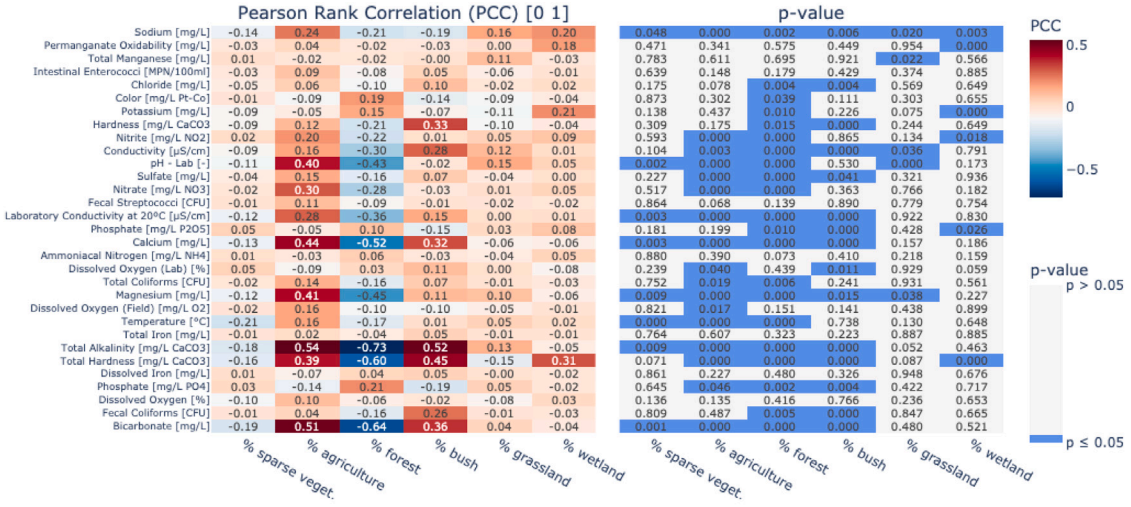

(a) Pearson correlation coefficient (PCC)

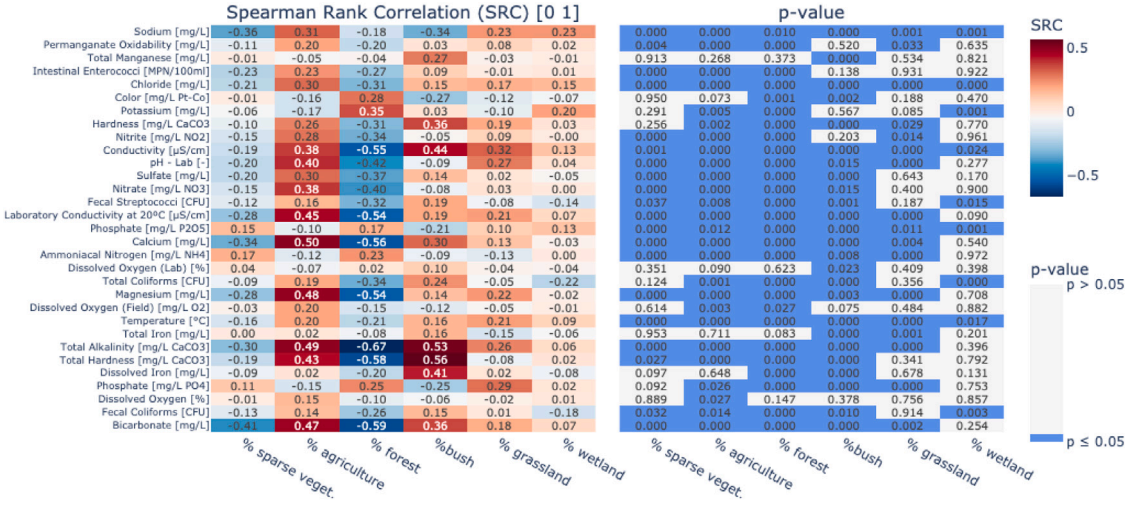

(b) Spearman's rank correlation coefficient (SRC)

Fig. 8. Correlation coefficients aggregated by river basins: (top) Pearson correlation coefficient (PCC), (bottom) Spearman's rank correlation coefficient (SRC).

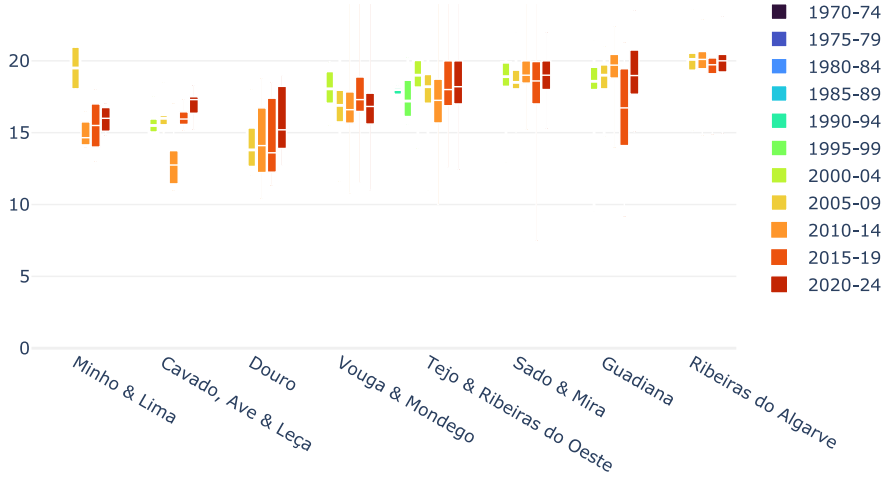

Fig. 9. Boxplot of groundwater temperature observations (°C) from 1970 to 2024, aggregated by river basin groups. The *x*-axis shows four hydrogeological units (eight river basin groups in total)

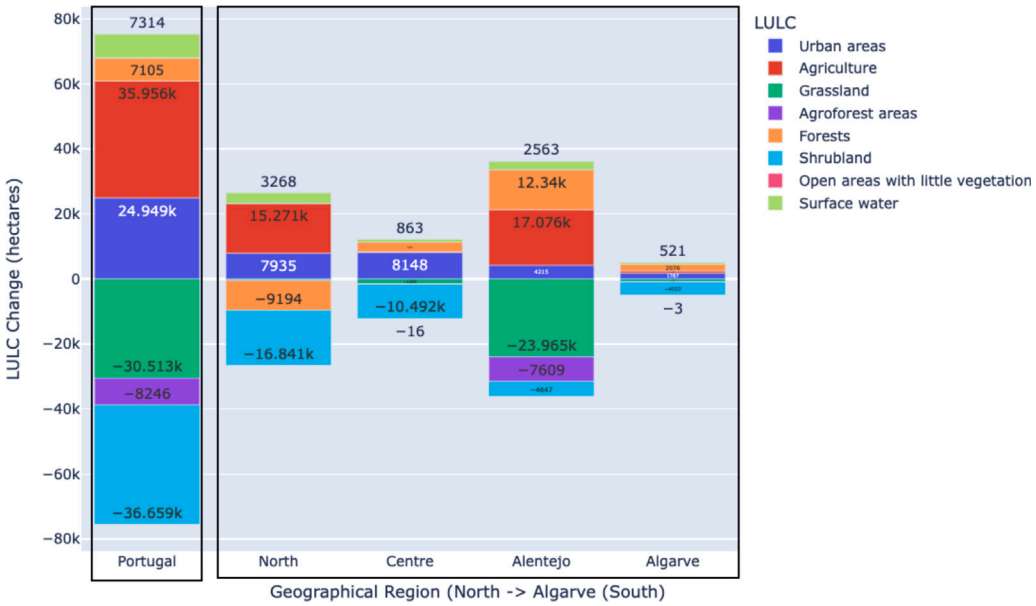

Fig. 10. Land Use and Occupation Chart (COScid) change between 2007 and 2018 (DGT, 2025).

supported by modelling projections and scenario-based analyses, potentially enhanced through the application of artificial intelligence and deep learning techniques.

To reduce and mitigate groundwater quality deterioration and depletion, the development and implementation of specific risk-based pollution management plans is encouraged to support policy-makers and water resources managers in developing the best strategies.

5. Conclusions

This study addresses a critical knowledge gap by presenting the first comprehensive assessment of large-scale, long-term groundwater status (quantity and quality) on mainland Portugal, covering four major hydrogeological units and 15 principal river basins. It aims to disentangle natural from anthropogenic controls, supporting more coherent, nationwide water management strategies in regions vulnerable to climate change and anthropogenic pressure. Findings are based on over 4.4 million observations spanning five decades.

Groundwater quality consistently declined from the cooler, wetter north to the warmer, drier south, with elevated electrical conductivity and chloride levels in southern regions reflecting evapoconcentration, geology, and limited recharge, revealing that natural climate effects intertwine with agricultural pressures. Seasonal variability was evident: nitrate and potassium levels typically rose during wetter months likely due to fertilizer mobilization, while pH and calcium remained more stable, consistent with geochemical buffering.

Long-term patterns show (i) stable water depth in northern units, (ii) signs of aquifer overexploitation and degradation in the south with potential occurrence of saline intrusion (Orla Meridional), (iii) declining nitrate in some areas since 2000, and (iv) no clear trends for phosphate. Disentangling climate-gradient-driven patterns from anthropogenic influences was key to identifying persistent degradation hotspots in intensively farmed zones, where poor groundwater quality persists despite the implementation of the basin management plans within the WFD since 2010. Agricultural land cover was more strongly associated with elevated Total Alkalinity, Total Hardness, Calcium, pH, Bicarbonate, Magnesium, Conductivity, and Nitrate; however, these patterns could only be partially explained by land use alone, highlighting the additional influence of lithology and soil type.

CRediT authorship contribution statement

Diogo Costa: Writing – review & editing, Visualization, Validation, Supervision, Software, Resources, Project administration, Methodology, Investigation, Funding acquisition, Formal analysis, Data curation, Conceptualization. **João Santos:** Writing – review & editing, Writing – original draft, Conceptualization. **António Chambel:** Writing – review & editing, Writing – original draft, Conceptualization.

Declaration of competing interest

The authors declare the following financial interests/personal relationships which may be considered as potential competing interests: Diogo Costa reports financial support was provided by Portuguese Foundation for Science and Technology. Diogo Costa reports financial support was provided by European Union. Diogo Costa reports financial support was provided by Water4All. If there are other authors, they declare that they have no known competing financial interests or personal relationships that could have appeared to influence the work reported in this paper.

Acknowledgements

This work was co-financed by the European Union and national funds through the Fundação para a Ciência e a Tecnologia (FCT), Portugal under the Water4All Partnership, within the ENGAGE project (Water4All/0003/2023). The authors acknowledge the R&D unit MED – Mediterranean Institute for Agriculture, Environment and Development (https://doi.org/10.54499/UIDB/05183/2020; https://doi.org/10.54499/UIDP/05183/2020) and the Associate Laboratory CHANGE – Global Change and Sustainability Institute (https://doi.org/10.54499/LA/P/0121/2020). The authors also acknowledge the financial support provided to the Institute of Earth Sciences (ICT), Portugal through the multi-annual funding contract with FCT (project UID/04683). Additionally, the PT team is co-funded by national funds through FCT, Portugal in the framework of the project UIDB/06107 – Centro de Investigação em Ciência e Tecnologia para o Sistema Terra e Energia (CREATE).

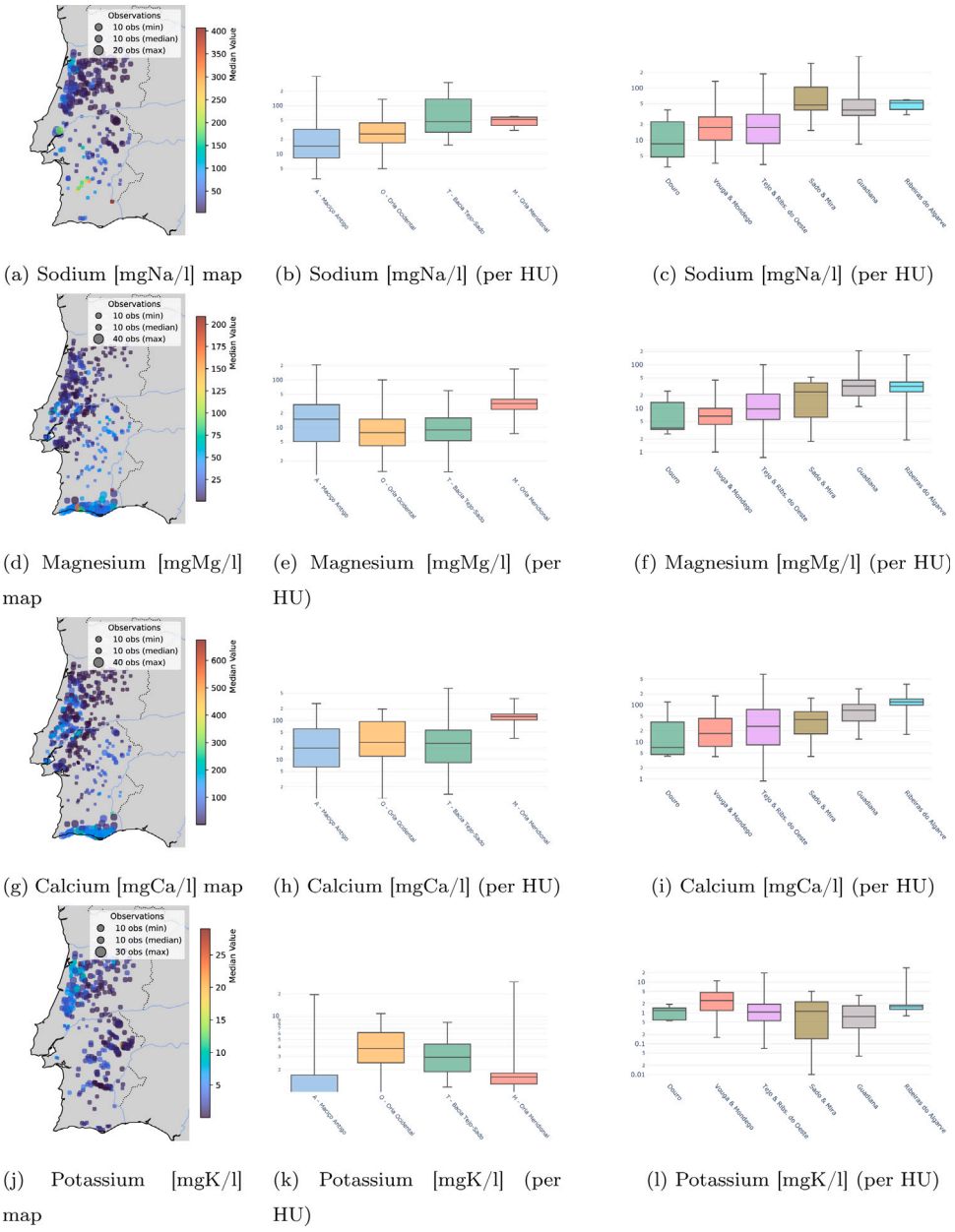

(a) Sodium [mgNa/l] map (b) Sodium [mgNa/l] (per HU) (c) Sodium [mgNa/l] (per HU)

(d) Magnesium [mgMg/l] map (e) Magnesium [mgMg/l] (per HU) (f) Magnesium [mgMg/l] (per HU)

(g) Calcium [mgCa/l] map (h) Calcium [mgCa/l] (per HU) (i) Calcium [mgCa/l] (per HU)

(j) Potassium [mgK/l] map (k) Potassium [mgK/l] (per HU) (l) Potassium [mgK/l] (per HU)

Fig. A.1. Median values of alkaline metals Sodium [mgNa/L], Magnesium [mgMg/L], Calcium [mgCa/L] and Potassium [mgK/L] are shown as spatial maps (left panels) and boxplots aggregated by HU (middle panels) and RB (right panels). Maps display the spatial distribution of each parameter, with circle colour indicating median values and size representing the number of observations. Aggregated groups are ordered along a north–south climatic gradient, from cooler, wetter regions to warmer, drier ones, reflected left to right on the x-axis.

Appendix. Spatial patterns for additional parameters

Fig. A.1 presents the median concentrations of alkaline metals, specifically Sodium [mgNa/l], Magnesium [mgMg/l], Calcium [mgCa/l], and Potassium [mgK/l]. These parameters are displayed as spatial maps (left panels) and as aggregated values by HU (middle panels) and RB (right panels).

The results reveal a clear southward increase in most alkaline metal concentrations, with the exception of potassium, which exhibits the opposite trend. These spatial patterns are consistent across both aggregation methods (hydrogeological units and river basins), but the gradient is more pronounced when aggregated by river basins. This stronger signal likely reflects the fact that river basins align more directly along a north–south gradient, highlighting geological influences, potentially reinforced by climatic factors.

Fig. A.2 presents the median values of Total Iron [mgFe/l] (acidic metal) and various minerals and salts, namely Chloride [mgCl/l], Sulphate [mgSO_4/L], and Calcium carbonate [mg$CaCO_3$/l]. These parameters are shown as spatial maps (left panels), and are also aggregated by HU (middle panels) and RB (right panels). The HU and RB are ordered geographically from north to south. While chloride and calcium carbonate show an increasing trend southwards, total iron and sulphate do not observe a clear tendency.

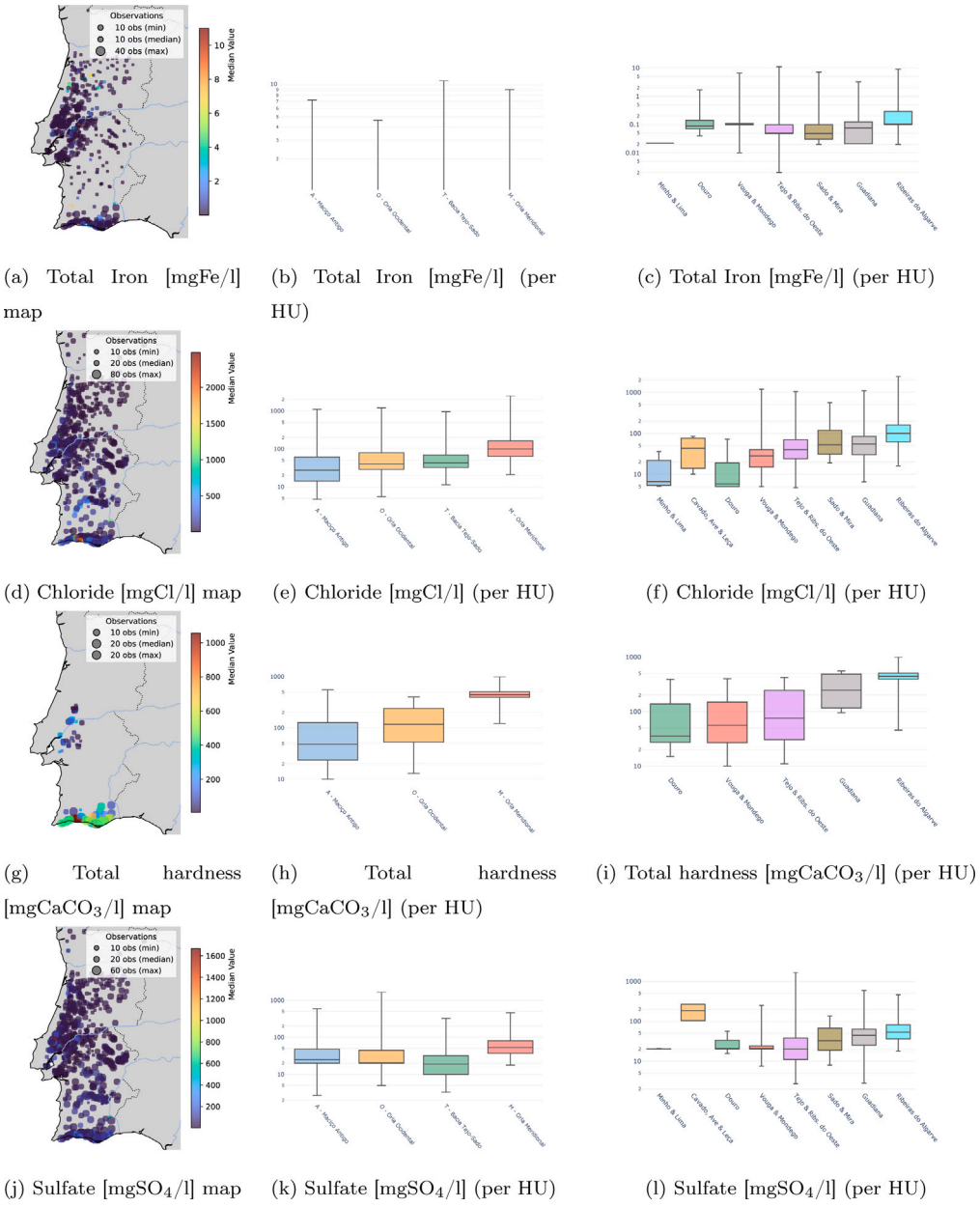

(a) Total Iron [mgFe/l] map (b) Total Iron [mgFe/l] (per HU) (c) Total Iron [mgFe/l] (per HU)

(d) Chloride [mgCl/l] map (e) Chloride [mgCl/l] (per HU) (f) Chloride [mgCl/l] (per HU)

(g) Total hardness [mgCaCO$_3$/l] map (h) Total hardness [mgCaCO$_3$/l] (per HU) (i) Total hardness [mgCaCO$_3$/l] (per HU)

(j) Sulfate [mgSO$_4$/l] map (k) Sulfate [mgSO$_4$/l] (per HU) (l) Sulfate [mgSO$_4$/l] (per HU)

Fig. A.2. Median values of acidic metal Total Iron [mgFe/L] and minerals Chloride [mgCl/L], Sulphate [mgSO$_4$/L], and Calcium carbonate [mgCaCO$_3$/L] are shown as spatial maps (left panels) and boxplots aggregated by HU (middle panels) and RB (right panels). Maps display the spatial distribution of each parameter, with circle colour indicating median values and size representing the number of observations. Aggregated groups are ordered along a north–south climatic gradient, from cooler, wetter regions to warmer, drier ones, reflected left to right on the *x*-axis.

Data availability

We have shared the link to the data and code in the manuscript.

References

Abduljaleel, Y., Amiri, M., Amen, E.M., Salem, A., Ali, Z.F., Awd, A., Lóczy, D., Ghzal, M., 2024. Enhancing groundwater vulnerability assessment for improved environmental management: addressing a critical environmental concern. Environ. Sci. Pollut. Res. 31 (13), 19185–19205. http://dx.doi.org/10.1007/s11356-024-32305-1.

Almeida, C., Lopo, M., Jesus, M., Gomes, A., 2000. Sistemas Aquíferos de Portugal Continental, vol. I. p. 133. http://dx.doi.org/10.13140/RG.2.1.1012.6160.

Bennett, J., 2010. OpenStreetMap. Packt Publishing Ltd.

Chung, S.Y., Kim, G.B., Senapathi, V., 2023. Drought and groundwater development. Water 15 (10), 1908. http://dx.doi.org/10.3390/w15101908.

Costa, D., Liu, J., Palma, P., 2025. Multidecadal water quality trends across 15 European river basins along a mediterranean climate gradient. Sci. Total Environ. 998, 180230. http://dx.doi.org/10.1016/j.scitotenv.2025.180230.

Costa, D., Sutter, C., Shepherd, A., Jarvie, H., Wilson, H., Elliott, J., Liu, J., Macrae, M., 2022. Impact of climate change on catchment nutrient dynamics: insights from around the world. Environ. Rev. 31 (1), 4–25. http://dx.doi.org/10.1139/er-2021-0109.

DGT, 2025. Land use and occupation chart (COScid).

European Environment Agency, 2022. Europe's Groundwater: a Key Resource Under Pressure. Publications Office, LU.

Eurostat, 2025. Irrigation: number of farms, areas and equipment by size of irrigated area and NUTS 2 region (2005 - 2013).

Feranec, J., 2016. Project CORINE land cover. In: European Landscape Dynamics. CRC Press, pp. 39–44.

Foster, S., Bjerre, T.K., 2022. Diffuse agricultural pollution of groundwater: addressing impacts in Denmark and eastern England. Water Qual. Res. J. 58 (1), 14–21. http://dx.doi.org/10.2166/wqrj.2022.022.

Frappart, F., Merwade, V.M., 2022. Editorial: Groundwater systems worldwide. Front. Earth Sci. 10, 1097789. http://dx.doi.org/10.3389/feart.2022.1097789.

Heberger, M., 2023. delineator.py: Fast, accurate watershed delineation using hybrid vector- and raster-based methods and data from MERIT-hydro. http://dx.doi.org/10.5281/zenodo.10143149.

Huang, G., Sun, J., Zhang, Y., Chen, Z., Liu, F., 2013. Impact of anthropogenic and natural processes on the evolution of groundwater chemistry in a rapidly urbanized coastal area, South China. Sci. Total Environ. 463–464, 209–221. http://dx.doi.org/10.1016/j.scitotenv.2013.05.078.

Huang, G., Zhang, M., Liu, C., Li, L., Chen, Z., 2018. Heavy metal(loid)s and organic contaminants in groundwater in the pearl River Delta that has undergone three decades of urbanization and industrialization: Distributions, sources, and driving forces. Sci. Total Environ. 635, 913–925. http://dx.doi.org/10.1016/j.scitotenv.2018.04.210.

Kaminsky, E., Englisch, C., Griebler, C., Steiner, C., Götzl, G., Knoeller, K., Sandén, H., Laaha, G., Stumpp, C., 2023. What are the driving factors affecting urban groundwater quality? A multi-tracer approach for the assessment of Vienna's shallow aquifers. http://dx.doi.org/10.5194/egusphere-egu23-5588, Publisher: Copernicus GmbH.

Kolpin, D.W., Barbash, J.E., Gilliom, R.J., 1998. Occurrence of pesticides in shallow groundwater of the United States: Initial results from the national water-quality assessment program. Environ. Sci. Technol. 32 (5), 558–566. http://dx.doi.org/10.1021/es970412g.

Kumar, A., Singh, A., 2024. Pollution source characterization and evaluation of groundwater quality utilizing an integrated approach of water quality index, GIS and multivariate statistical analysis. Water Supply 24 (10), 3517–3539. http://dx.doi.org/10.2166/ws.2024.213, Publisher: IWA Publishing.

Mansilha, C., Melo, A., Martins, Z., Ferreira, I., Maria Pereira, A., Espinha Marques, J., 2020. Wildfire effects on groundwater quality from springs connected to small public supply systems in a peri-urban forest area (Braga region, NW Portugal). Water 12 (4), 1146. http://dx.doi.org/10.3390/w12041146, Publisher: MDPI AG.

Meghanad, U., Vasanthamohan, V., Selvakumar, S., 2025. Groundwater quality assessment for drinking and irrigation: A case study in the cauvery river Basin (CRB) of tiruchirappalli district, Tamil Nadu, India. Water Qual. Res. J. 60 (1), 73–88. http://dx.doi.org/10.2166/wqrj.2024.031, Publisher: IWA Publishing.

do Nascimento, T.V.M., de Oliveira, R.P., Condesso de Melo, M.T., 2024. Impacts of large-scale irrigation and climate change on groundwater quality and the hydrological cycle: A case study of the alqueva irrigation scheme and the Gabros de Beja aquifer system. Sci. Total Environ. 907, 168151. http://dx.doi.org/10.1016/j.scitotenv.2023.168151.

Patekar, M., Baniček, I., Rubinić, J., Lukač Reberski, J., Boljat, I., Selak, A., Filipović, M., Terzić, J., 2021. Assessing climate change and land-use impacts on drinking water resources in karstic catchments (southern Croatia). Sustainability 13 (9), http://dx.doi.org/10.3390/su13095239.

Penha, A.M., Chambel, A., Murteira, M., Morais, M., 2016. Influence of different land uses on groundwater quality in southern Portugal. Env. Earth Sci. 75 (7), 622. http://dx.doi.org/10.1007/s12665-015-5038-7.

Portela, M.M., Espinosa, L.A., Zelenakova, M., 2020. Long-term rainfall trends and their variability in mainland Portugal in the last 106 years. Climate 8 (12), http://dx.doi.org/10.3390/cli8120146.

Rocha, J.L., Oliveira, V., Dias-Ferreira, C., 2019. Phosphorus flows in the portuguese agriculture and livestock sectors. In: Wastes: Solutions, Treatments and Opportunities III. pp. 434–439. http://dx.doi.org/10.1201/9780429289798-68.

Santos, J.F., Carriço, N., Miri, M., Raziei, T., 2025. Distributed composite drought index based on principal component analysis and temporal dependence assessment. Water 17 (1), http://dx.doi.org/10.3390/w17010017.

Shaikh, M., Birajdar, F., 2024. Groundwater and ecosystems: understanding the critical interplay for sustainability and conservation. EPRA 181–186. http://dx.doi.org/10.36713/epra16111.

Van Huijgevoort, M.H.J., Voortman, B.R., Rijpkema, S., Nijhuis, K.H.S., Witte, J.P.M., 2020. Influence of climate and land use change on the groundwater system of the Veluwe, The Netherlands: A historical and future perspective. Water 12 (10), http://dx.doi.org/10.3390/w12102866.

Yamazaki, D., Ikeshima, D., Sosa, J., Bates, P.D., Allen, G.H., Pavelsky, T.M., 2019. MERIT hydro: A high-resolution global hydrography map based on latest topography dataset. Water Resour. Res. 55 (6), 5053–5073. http://dx.doi.org/10.1029/2019WR024873.

Zeferino, J., Carvalho, M.R., Lopes, A.R., Jesus, R., Afonso, M.J., Freitas, L., Carvalho, J.M., Chaminé, H.I., 2021. Assessment of future trends on groundwater quality in a nitrate vulnerable zone (Esposende–Vila do conde sector, NW Portugal): towards a combined conceptual and mass transport modelling. Hydrogeol. J. 29 (6), 2267–2283. http://dx.doi.org/10.1007/s10040-021-02368-2, Publisher: Springer Science and Business Media LLC.

Zhang, F., Huang, G., Hou, Q., Liu, C., Zhang, Y., Zhang, Q., 2019. Groundwater quality in the pearl River Delta after the rapid expansion of industrialization and urbanization: Distributions, main impact indicators, and driving forces. J. Hydrol. 577, 124004. http://dx.doi.org/10.1016/j.jhydrol.2019.124004.